

Traineeship Report

« Theia: a Novel 3D Gaussian Beam Tracer »

Raphaël Duque

Traineeship advisor: Dr. Antonino Chiummo
Traineeship period: April 5th to August 25th 2017

European Gravitational Observatory
Via Edoardo Amaldi Santo Stefano a Macerata, Cascina
Pisa, Italia

Riconoscimenti

It is safe to say than none of this work would have been possible without the positive environment of Virgo and the positive input coming from all sides I had the chance to benefit from. Before entering the core of this report, I like to show my recognition to all the actors of this environment.

First off, I would like to thank my advisors Antonino Chiummo and Éric Genin, who have introduced me to the world of gravitational interferometry, its people, its physics and its methods in a smooth way and with much perspective on all the disciplines gathered in interferometry. They have always overseen the progress of our project with benevolence and rigor, never left me in doubt and when needed pointed me to the appropriate resources. I formulate the wish that our work may continue in the future and that our collaboration may be fruitful to astronomy.

J'aimerais montrer ma reconnaissance à Gabriel Pillant, car il m'a introduit pratiquement à l'optique de Virgo, m'y a laissé participer un tant soit peu, et m'a conseillé ça et là pour rendre notre programme facile d'usage et effectivement utile au laboratoire d'optique.

Ensuite je remercie les autres stagiaires Léa Lhopital, Benjamin Rémy, David Cohen, Nathan Flood, ainsi que Camilla de Rossi et Matthieu Gosselin qui au-delà d'avoir fourni des conversations animées de physique à l'observatoire se sont révélés des amis pisans (pour ne pas dire des compagnons d'aventure), et pour l'avenir des premières connaissances de mon âge de l'univers de l'astronomie gravitationnelle.

Ringrazio di cuore Andrea Magazzù per avere avuto una posizione accogliente e per i suoi insegnamenti sul software 3D, e tutte le componenti che ne fanno una parta importante del nostro progetto.

Ringrazio la mia diretta collega e compagna di lavoro Annalisa Allocca per il suo supporto e per essere stata capace di venire a patti con il mio italiano e il mio fischio.

Inoltre, vorrei manifestare la mia riconoscenza per Carlo Bradaschia, per la sua storica intuizione sull'interferometria gravitazionale di Pisa, per avermi condotto alle fonti primarie della parte storica de questo rapporto.

Finally, I must warmly thank all the people in and out of the interferometry community who have contributed to our endeavor by suggesting features, algorithms, ideas on the communication and documentation of our project, those who have found the name, the best design for the public interface, provided enthusiasm and helped to drive the project from afar. They make this project a wide collaboration and the list of all of these contributors is to long to detail here but would most certainly start with the names of Gabriel Duque, Hiro Yamamoto, Gary Hemming and Yoichi Aso.

Resumé

Nous rapportons le développement, les essais et les premiers cas d'usage d'un nouveau logiciel de simulation de faisceaux gaussiens en trois dimensions auprès de l'interféromètre gravitationnel Virgo. Le contexte d'observatoires gravitationnels et en particulier la nature de l'activité liée à l'optique qui s'y déroule exige que les logiciels disponibles possèdent certaines fonctionnalités précises. Celles-ci comprennent la possibilité d'automatisation personnalisée des tâches en plus de l'usage de l'outil tel quel, la simulation des faisceaux gaussiens astigmatiques généraux, le calcul des interférences, la visualisation dynamique et tridimensionnelle des faisceaux simulés parmi les éléments des bancs optiques, et la navigation aisée parmi les faisceaux simulés à la recherche de faisceaux parasites. Ces exigences sont imposées par la physique et les méthodes de l'interférométrie gravitationnelle. Nous décrivons les outils existants afin de motiver le développement d'un nouvel outil. Le nouveau programme `theia` est décrit des points de vue optique et algorithmique avec la perspective de ces exigences. Le nouveau logiciel révèle ses capacités dans le cadre de premiers cas d'usage rencontrés lors de la mise en place de l'interféromètre *Advanced Virgo*. Lors du traitement de ces premiers cas, les capacités de la bibliothèque `theia` et le potentiel de simulation de `theia` sont exhibés, et des considérations de performance dans des simulations à l'échelle de Virgo sont faites. Un environnement utilisateur à `http://theia.hopto.org` a été conçu pour supporter le nouveau programme.

Summary

We report the development, testing and first use cases of a new 3-dimensional Gaussian beam tracing simulation software at the Virgo gravitational interferometer. The context of gravitational observatories and specially the nature of the optical activity therein require that the available simulation software provide peculiar functionalities. These are scripting capabilities alongside the standalone command line tool, the simulation of general astigmatic Gaussian beams, the calculation of interferences, dynamical 3-dimensional rendering of the simulated beams among the optical setup and the easy navigation through the set of the generated beams in search for stray beams. These requirements are advocated by the physics and methods of gravitational interferometry and the pre-existing tools are reviewed in motivation of the new tool. The new software `theia` is described from the optical and computational points of view as it attempts to meet these requirements. It reveals its capabilities in some first use cases encountered during the commissioning of the Advanced Virgo observatory. With these use cases, both the scripting capabilities of the `theia` library and the simulation potential of the command line tool are exhibited, and some considerations of the performances of the software in Virgo-scale simulations are made. A user environment at `http://theia.hopto.org` has been built to support the new program.

Foreword

Here we will report the first phases of development, testing and using of the `theia` tool. It is of importance to acknowlege that this software is a live project, of which the final version is ambitious and is not likely to be released soon.

Consequently, an important effort has been made in order for the project to be carried on in the future by other teams. Its complete and formal description is written as we go along and is intended to be read by future contributors for the sake of dynamism in the life of the project. This description largely oversizes the content of this report, and was evidently never intended to be included here. It can be found on the project's website at `http://theia.hopto.org` along with vast written and online documentation, releases, tutorials and instructions for obtaining the live sources.

We are in the hope that these months were but the beginning of a long and healthy life for the `theia` Project and invite all contributors in and out of the gravitational astronomy community to join efforts for the progress of gravitational interferometry and computation therein.

Cascina, August 24^{th} 2017

Contents

Summary . . . ii
Foreword . . . iii

Introduction **2**

1 The physics and detection of gravitational waves **3**
1.1 A bit of history and the detection challenge . . . 3
1.2 Perspectives of gravitational astronomy and the interferometer network . . . 5
1.3 The astrophysics and cosmology of gravitational waves . . . 6

2 Principles of gravitational interferometry **9**
2.1 Signal and noise . . . 10
2.2 The simple shot noise limited Michelson interferometer. . . . 11
2.3 Introduction to the optical layout of Advanced Virgo . . . 14

3 The optics of gravitational interferometry **16**
3.1 3D setups and astigmatic Gaussian beams . . . 16
3.2 The optics context of gravitational observatories and requirements for new software 19
3.3 Current solutions for simulation . . . 21

4 `theia`: a new tool for gravitational observatories **22**
4.1 The theia rationale . . . 22
4.2 The operation of theia . . . 23
4.3 Beams and optics . . . 23
4.4 Algorithm and approximations . . . 24
4.5 Schedule of `theia` . . . 25

5 Benchmarking and first steps **26**
5.1 Performances of the software . . . 26
5.2 Thermal lensing investigation at Virgo . . . 28
5.3 Optical bench designing . . . 28

Conclusions and perspectives **30**

Introduction

Gravitational waves are an early prediction of Albert Einstein's theory of General Relativity. Gravitational interferometry is an emerging method of gravitational astronomy, and aims at detecting and characterizing the transient signals induced by the passage of a gravitational wave on the laser light introduced inside a kilometer-scaled optical interferometry setup. This method is implemented mainly in the two observatories of the American LIGO Scientific Collaboration and in the French-Italian Virgo observatory near Pisa, Italy. Gravitational interferometry culminated in these last two years as three gravitational wave signals were detected by the LSC-Virgo Collaboration. They most likely were emitted by the coalescences of binary stellar black holes in distant galaxies.

Gravitational interferometry demands the convergence of a large pool of skills, as it consists in designing and realizing a complex optical setup and various detection instruments, isolating these instruments from environmental noise, identifying and attenuating these noises in the use of servo loops actuating on all components of the observatory in order to maintain the interferometer in a state of maximum sensibility. Gravitational interferometry also requires a great deal of data extraction and analysis.

The field of Gaussian optics – the study of the spectral content and of the interaction with optical components of Gaussian-shaped light beams, in practice those produced by lasers – is of first importance in gravitational interferometry. Indeed, the optical setups such as those of the Virgo observatory seek to measure and interpret the interference pattern at the output of a Michelson-type interferometer, this interferometer having been fed with a Gaussian light beam of which the spectral characteristics are as precisely determined as possible. Thus, one of the main scopes of Gaussian optics in this context is the treatment of the bare laser-output beam in order to purify its frequency and spatial mode spectra, before injecting it in the interferometer itself.

What's more, the numerical simulation of Gaussian beams plays a fundamental role in the conception and realizing of optical benches. This is because of the scale of kilometer-large optical setups, the effects of Gaussian optics are felt, and the precision demanded by gravitational interferometry requires that any sub-system be thoroughly tested, and thus simulated beforehand.

In this work be report the development and testing of a new Gaussian optics simulation software, `theia`, at the Virgo observatory, to be used by the gravitational interferometry community as a whole, and which responds to the constraints of this activity. This new program benefits of an extensive user environment at `http://theia.hopto.org`.

We will first overview the physics of gravitational waves and of their detection. This will lead us to detail the principles of gravitational interferometry and its optical context. This will motivate the development of a new tool, which we will then briefly present, ending with the description of the first cases the new software has treated.

1 The physics and detection of gravitational waves

1.1 A bit of history and the detection challenge

From GR to the indirect observation of GW. Gravitational waves were an early prediction of Albert Einstein's theory of General Relativity (GR). GR is a formulation of the gravitational interaction in terms of the deformation of the fabric of space-time, and solves many fundamental problems inherent to Isaac Newton's theory of gravitation, the first of which are the instantaneous and remote action of gravity, and the decoupling of gravity to all massless objects such as photons and light. In the theory of GR, space-time is a continuous and deformable medium, the curvature of which is constrained by the local content of energy and momentum with a coupling constant of the order of $8\pi G/c^4 \sim 10^{-43}$ s^2/kg.m . This is explicit in Einstein's field equations, a set of 10 non-linear coupled partial differential equations linking the so-called Einstein tensor which encompasses the geometrical information of space-time and the stress-energy tensor, which contains the dynamical information on the physical content of space-time.

Upon linearization around the flat space-time solution (corresponding to the empty and flat Universe), the Einstein equations give rise to wave equations. These wave equations were derived in Albert Einstein's founding article of 1916 ([7]) and directly interpreted as the stationary regime propagation in vacuum at the speed of light of a perturbation of the metric.

Shortly after in 1918 ([9]), Einstein derived to leading order the structure of the GW emitted by a *non-self-gravitating source*, i.e. that of a test mass in an external field. This revealed the quadrupolar nature of GW radiation, as it is expressed as the second time derivative of the Newtonian mass quadrupole of the source. It was then noted that the quadrupolar nature of GW implies that sources cannot posses a spherical symmetry – as it is the case of many astrophysical objects.

This result was found by Lev Landau and Evgeny Lifshitz in 1941 ([8]) to be extensible to the case of *self-gravitating* sources, i.e. sources considered in motion in their own gravitational field. The astrophysical archetype of self-gravitating systems are binary systems such as binary stars or binaries of then-very-controversial neutron stars.

Considering a circular binary system of point masses and equating the flux at infinity of the GW radiation emitted by the system (as Einstein had derived it in 1918) with the loss of gravitational potential energy – in fact the binding energy –, one is led to an ordinary differential equation on the so called *secular* evolution of the radius of the system in time. It is found that by GW radiation, the two members of the binary system will inevitably converge and eventually their relative distance will formally vanish after a *finite* time of coalescence. This is the formal description of a merger by GW radiation.

Freeman Dyson is explicit on the consequences of this coalescence in the case of a binary neutron star in 1963 (from [10]):

"According to [the Einstein-Landau-Lifshitz quadrupole formula], the loss of energy by gravitational radiation will bring the two stars closer with ever-increasing speed, until the last second of their lives they plunge together and release a gravitational flash at a frequency of 200 cycles and of unimaginable intensity."

This vision of Dyson was concretely realized in the spectacular observation by Russell Hulse and Joseph Taylor in 1973 of the orbital decay of PSR B1913+16, a binary of neutron stars one of which one is a pulsar ([11]). Radioastronomy methods allowed them to determine the pulse period and thus the orbital period of the system. This orbital period was found to decrease systematically and within an agreement of about 0.3 % with the orbital decay predictions of GR by GW radiation. This astonishingly precise agreement is illustrated in figure 1. This work owed Hulse and Taylor the Nobel Prize in 1993 "for the discovery of a new type of pulsar, a discovery that has opened up new possibilities for the study of gravitation." The calculated lifetime of PSR B1913+16 before merger is 300 million years.

Gravitational radiation from binaries are today the most important sources for GW detection. Pulsar timing as pioneered by Hulse and Taylor is an active domain for the search for GW signals, as in projects such as the European Pulsar Timing Array and the North American Nanohertz Observatory for Gravitational Waves.

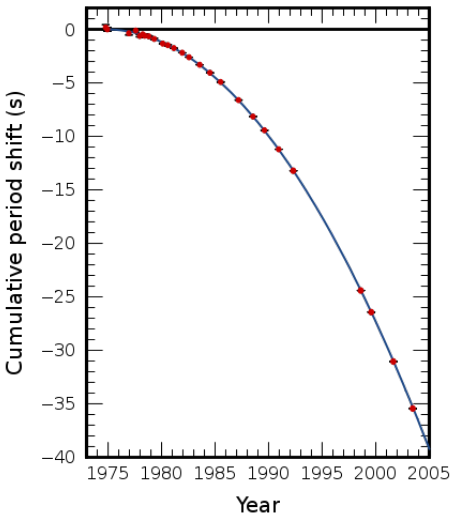

Figure 1: The orbital decay of PSR B1913+16 according to Hulse and Taylor's radio observations (red points), along with the predictions of GR by GW radiation (continuous blue line, from [11]).

The challenge of direct detection. At that moment, the existence of GW was indirectly proved. Thus the physical reality of GW was assured and the direct detection of GW became a matter of designing, building and commissioning a dedicated instrument capable of detecting GW as directly as possible.

Gravitational interferometers such as the American Laser Interferometer Gravitational-Wave Observatory (LIGO) and the French-Italian Virgo are such instruments. Gravitational interferometers use the effects of GW on the propagation of light in order to detect the passage of GW. We will detail this mechanism in further parts of this report.

The fundamental ideas of gravitational interferometers are to introduce the light from a laser source of which the spectral content is known (or *controlled*) as precisely as possible into an optical interferometry setup of which we know (or *control*) the rest (or *static*, i.e. in the absence of a GW) position as precisely as possible, in order to measure the variation of distances within the optical setup induced by the passage of a GW. This implies the knowledge and attenuation of all possible noises in the setup and the laser, and is thus relevant to an extremely large spectrum of fields of physics and engineering, from optical design to vacuum control and from data analysis to electro-mechanic control systems.

The Virgo gravitational interferometer is the instrument designed and commissioned by an international collaboration in Cascina, Italy. This collaboration was historically founded (see [17] for a detailed historical review) by Alain Brillet of the University of Orsay and colleagues from Paris VI University and the *Centre National de la Recherche Scientifique* (CNRS), and Adalberto Giazotto of the University of Pisa and colleagues from the *Instituto Nazionale di Fisica Nucleare* (INFN).

Brillet and his team had by 1985 reviewed many optical designs for gravitational interferometry, including the expected noises linked to the laser source, the study of mirror quality linked issues, and mode cleaners. Concentrating on shot and laser noise, a broad work had been led on high power and high stability lasers, coupled with recycling techniques as suggested by Ron Drever. In 1989 a prototype of injection locked Nd-YAG laser reached a world record of 18 W. This opened the perspective of a highly controlled laser source for a gravitational interferometer.

In the meantime, Giazotto gathered a group of collaborators around the idea a detecting GW in bands as low as 10 Hz, as suggested by radio astronomy discoveries of low-orbital frequency pulsars. In this band, the limiting noise for position control of an experimental Earth-bound setup is seismic noise. The idea of controlling a suspended object's position in six different degree of liberty by a cascade of pendulums composed of heavy test masses and controlled by piezoelectric actuators in a servo loop emerged. These *superattenuators* would be the core of any eventual

gravitational interferometer's seismic noise control system.

In 1985 Giazotto and Brillet met as Giazotto presented his work at the 4^{th} Marcel Grossman Meeting on GR in Rome. They realized the complementarity of their work and started working on a proposal to the CNRS and INFN of a collaboration to design, build and commission a 3 km-long gravitational interferometer, supported by both of their results in their own domains. The proposal was made in 1989 and accepted in 1994. The Virgo interferometer was built between 1996 and 2003, and joint observing runs began with the LIGO interferometers which had attained their full sensitivity in 2005. As of 2011, the Advanced Virgo project aiming at increasing the sensitivity of the interferometer started. The commissioning of Advanced Virgo is currently reaching its goal.

1.2 Perspectives of gravitational astronomy and the interferometer network

For the sake of statistical significance and pinpointing the source of GW, it is necessary that gravitational observatories form a network of instruments, oriented in diverse directions and separated in space. In the near future, the gravitational interferometry network will likely be composed of the two LIGO detectors, the Virgo interferometer and the emerging interferometer of the Japanese KAGRA collaboration.

The future will also comprise of several LIGO-Virgo-like interferometers such as INDIGO in India or AIGO in Australia, as well as of new generation of ground-based instruments such as the underground triangle-shaped interferometer Einstein Telescope and possibly of space-bound instruments such as the LISA project.

The members of the future gravitational interferometry network are detailed in table 1.

Instrument	**Beginning of service**	**Frequency range** (Hz)	**Sensitivity** (peak, strain)	**Features**
Advanced Virgo	2017	$10 - 10\,000$	$10^{-23.7}$	3 km arms
aLIGO	Nov. 2016 (O2 run start)	id.	$10^{-23.8}$ (BNS-optimized)	4 km arms
KAGRA	2017 (pro.)	sim.	sim.	Under-ground, cryogenized test masses
Einstein Telescope	2025?	$10 - 10\,000$	$10^{-24.5}$	Under-ground, 10 km arms, triangular topology
LISA	2034	$10^{-3} - 1$	10^{-22}	Space-bound, $\sim 10^6$ km arms, triangular topology

Table 1: The future gravitational interferometry network (source: [12, 6, 19, 20]).

Gravitational observatories in the scope of astronomy. Finally, let us mention the integration of gravitational observatories in the landscape of astronomy, along with optical, near-optical, radio, gamma-ray, astroparticle, etc. observatories. As GW detectors are non-directional (they receive signals from all directions, similarly to astroparticle detectors), they may be viewed as *watch-outs* for the entire sky and may notify other astronomical facilities to observe in a given direction for a transient signal if one has been detected through a gravitational signal.

What's more, the gravitational spectrum is so large and is flown through during a single merger. Thus one may imagine a scenario in which the low frequency secular inspiral of a binary is picked up by a low frequency instrument such as LISA, before the merger which was thus predicted and awaited for in the acoustic band. After the detection of LISA, the signal gradually builds in the

acoustic band, to which the ground-based instruments are sensitive. The merger then occurs and in the mean time, gamma-ray observatories and other instruments may point to the relevant direction and gather all the information on the event in their own sectors.

Much as the cooperation between optical, X-ray and neutrino observatories allowed to make the most of supernova SN1987a, gravitational observatories may further participate in the global astronomy cooperation.

1.3 The astrophysics and cosmology of gravitational waves

Astrophysical and cosmological phenomenon may be sources of GW which carry information on the physical conditions of the phenomena. In this section we will motivate the detection of GW and introduce the sources and characteristics of these waves, as well as the information they may carry.

This goal of gravitational astronomy has been the main interest of all collaborations since the start. From the VIRGO Project Proposal ([17], September 1991):

"Considering that the detection of gravitational waves would provide:

- in the field of fundamental physics:
  - a direct proof of the existence of gravitational radiation
  - a proof of the tensor character of the gravitational field
- in the field of astronomy and astrophysics:
  - new means of observing distant objects, the third means besides electromagnetic waves and neutrinos: this new means of observation will be unique for highly energetic phenomenon such as collapses of supernovae and close binaries"

Multi-message astronomy. The principal scope of gravitational astronomy is *multi-message* astronomy, whereby the physical phenomena occurring within astrophysical objects are correlated by signals in many parallel channels: electromagnetic radiation, particles, etc. Up until now, multi-message astronomy has reposed on the electromagnetic spectrum and the detection of astroparticles. These two channels allow access to information such as the amount of energy released in each channel by the phenomena, and an insight on the thermonuclear and chemical equilibria at play in the phenomena. Figure 2 illustrates the multi-message astronomical study of the Sun, with the Sun in seen in X-rays presenting the magneto-hydro-dynamic phenomena in the solar corona, and the Sun seen in neutrinos, correlating the thermonuclear *pp* process at the heart of the Sun. The Sun's region under its photosphere is unaccessible to X-rays, and *vice-versa* neutrinos are not (though to be) produced by the star's photosphere.

GW will bring a third degree of liberty to multi-message physics, and one that is more *orthogonal* to the two others. The gravitational field is affected by the presence of energy, regardless of the form of that energy. GW are thus a universal messenger of all astrophysical phenomena, as long as the phenomena respects the quadrupolar symmetry of these waves. What's more, GW scarcely scatter with ordinary matter, and thus travel through space-time unaffected, conveying the message of their source until detection with little loss of information. Finally, GW have an extremely large spectrum as we will soon describe, and most importantly, there is no correspondence between the nature of a source and the part of the spectrum in which it lies. The signal emitted by a binary system traverses the GW spectrum from the mHz scale to the acoustic range from the inspiral phase to the the merger, the overall signal having an important presence in all parts of the GW spectrum, as illustrated by figure 3.

On the contrary of GW, it is traditional to name an celestial object by the band of the electromagnetic spectrum it primarily emits in, which leads to denominations such as Cyg X-1 or Low Mass X-ray Binary for an X-ray source, or Quasi Stellar Radio Source (quasar). In GW astronomy, a broad spectrum is covered by every source along its evolution in time.

A historical example of GW (seemingly) entering multi-message astronomy is that of supernova SN1987a in the Large Magellanic Cloud. During this event, the electromagnetic and the neutrino signals were correlated and confirmed the predicted energy distribution of a type II supernova as

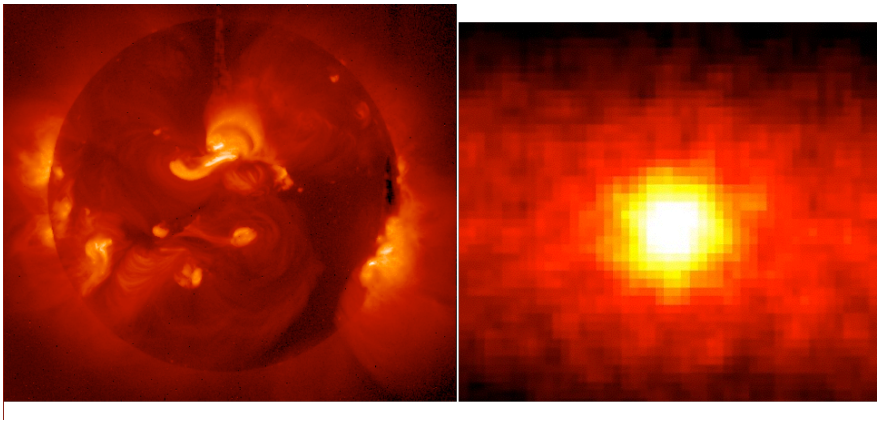

Figure 2: Left: the Sun in X-rays (Yohkoh Solar Satellite), right: the Sun in neutrinos (Super-Kamiokande Neutrino Detector). The neutrino image was obtained after 500 days of integration. Notice the Milky Way's disk in the background of the neutrino image. Two images not to scale.

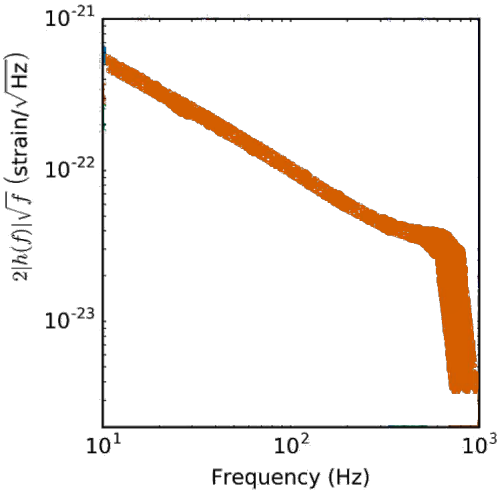

Figure 3: The spectral density of the merger signal of two stellar black holes (adapted from [6]). Data for the GW151226 event.

well as the existence of two other generations of leptons comprising the μ and τ neutrinos [13]. Joseph Weber, father of the Weber bar gravitational wave detectors, claimed to have detected GW from SN1987a, a claim which was received with skepticism by the astrophysical community.

In more recent events, the first GW detection by the LIGO-Virgo collaboration appeared to coincide with a gamma-ray burst as reported by the Fermi GBM collaboration in [16], in a region of the sky overlapping the uncertainty area of the origin of the GW event. Though gamma-ray bursts are not expected from this sort of event (black hole mergers) and the correlation between the burst and the GW signal is doubtful accoring to other teams ([14, 15]), this event does inaugurate gravitational astronomy as an emerging player of multi-message astronomy.

Binary systems. One of the most commonly expected sources of GW (and the only sources detected to date) are binary system coalescences, and most importantly those of black holes and neutron stars. Thus GW signatures of compact objects will likely shed light on the astrophysics of these binaries.

The black hole population is thought to be divided in two main sub-populations: stellar black holes and supermassive black holes. The former are thought to be formed by the gravitational

collapse of aged stars of masses in the range of $\sim$ 5–10 $M_\odot$, and the former to lie in the center of galactic nuclei and to have masses much larger than 10^5 $M_\odot$.

Using accurately calculated templates of the signal emitted by the coalescence of black holes, one is able to filter out the optical signal of a gravitational interferometer and extract the signal of a GW, if any. These templates are produced by a combination of numerical relativity computations and post-Newtonian analytic expansions, as extensively explained by Thibault Damour in [4]. During the first scientific run of the LIGO instruments, a collection of 250 000 such templates were used to identify GW signals. As the theory of the population of black holes predicted, the larger part of the templates used corresponded to the merging of black holes of masses in the range 1–30 $M_\odot$, with a large concentration under 4 $M_\odot$. The distribution of these templates is illustrated figure 4.

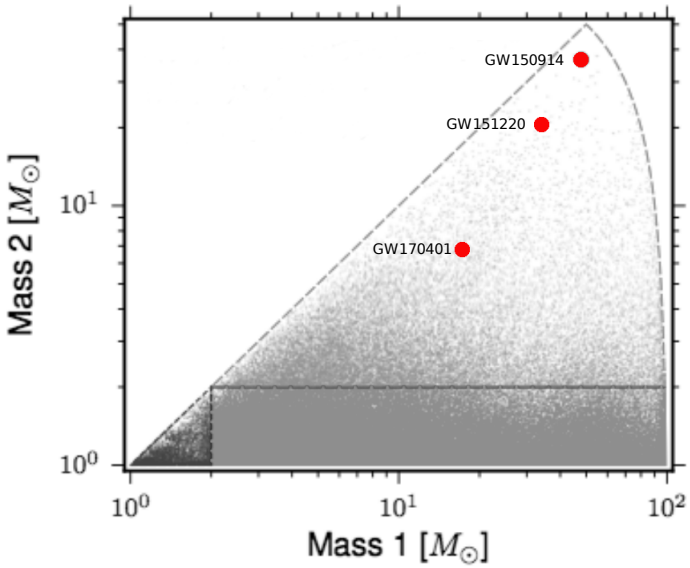

Figure 4: The templates used in current scientific runs for the search of binary black hole mergers. Each point represent a template fitted to a binary black hole with masses M_1 and M_2. The red points correspond to the binaries of the three first detections (data from [1, 2, 3]).

As one may infer from this figure, the three first detections concerned black holes out of the expected range, with masses of the order of $\sim$ 20 $M_\odot$. Thus gravitational astronomy has already brought information of the population of black holes in our (close) Universe. Moreover, observation of these mergers provide insight on the alignment and spins of the members of the binary, as these parameters are also included in the signal templates. Of course, information such as the merger rate in the detectable Universe can also be derived from gravitational astronomy events.

Due to the current number of detections, statistical significance is still to be improved. Nonetheless, we can expect a large increase of our knowledge of binary systems, and possibly a change in the accepted model of formation of binary systems, the alignment of their members, their existence in the heart of star clusters, and thus the age of these clusters, their composition and dynamics.

Primordial GW and cosmology. We will follow here the excellent development of Michele Maggiore in [5].

In the Standard Model of Cosmology, the Universe is regarded as a fluid distributed in a space-time which is subject to metric expansion. One consequence of this hypothesis is that as the Universe expands, the matter and energy densities decrease, modifying the equilibrium of the four fundamental forces. Namely, the equilibrium of two interacting components of the primordial plasma is maintained when the increase of concentration of a given species due to the interaction is compensated by the dilution of the species induced by the expansion of the metric. The expansion of the Universe is measured by the Hubble (time-varying) constant $H(t)$. The equilibrium of a

reaction is maintained as long as the rate Γ of the reaction is larger than $H(t)$. When this condition is no longer fulfilled, particles of one species of the reaction can propagate freely, because the other component's concentration is decreased by the expansion in such a way that the scattering of one on the other no longer occurs. The species are thus said to *decouple* and the particles of this *last scattering surface* carry information on the epoch of their decoupling, because the information is no longer altered by any further interaction.

In the case of the electromagnetic interaction, the equilibrium of photons, baryons and electrons is maintained by Compton scattering $H+\phi \rightarrow e^- + p$ and Coulomb scattering $e^- + p \rightarrow H$. Photons will decouple from the primordial hydrogen when $H(T_{\text{decouple}}) = \Gamma(T_{\text{decouple}})$, where the rate Γ in this case is $\sigma_T n_e$, σ_T being the temperature dependent Thompson scattering cross-section and n_e the concentration of free electrons, and the photon concentration is proportional to T^3. This condition leads to the well known Cosmic Microwave Background (CMB), composed of the photons emitted by the last scattering surface. We deduce that $\sim 400\,000$ years after the Big Bang, photons decoupled from ordinary matter and the photons of the CMB carry information on the state of the Universe at this epoch, and light cannot carry information on earlier epochs. This *Recombination* is the end of the *Photon epoch*.

In the case of the weak interaction, the cross section is proportional to Fermi's constant G_F and neutrinos decouple from leptons ~ 1 s after the Big Bang, leading to a cosmic neutrino background.

In the case of gravitation, the cross section is analogously proportional to Newton's constant, and it can be found that gravitons decouple from all the other components of the primordial plasma at energies below the Planck scale $T \sim 10^{19}$ GeV $\sim 10^{-43}$ s. This epoch is significantly earlier than the two previous decoupling epochs. It follows that the so-called *Stochastic GW Background*, emitted at this epoch carries information on this epoch onwards to the future in their frequency, amplitude, etc. and may be relics of the *very* high-energy conditions of the primordial Universe. Theoretical calculations can be led on this GW background, and their frequency is thought to typically lie around 10^{-7} Hz ([18]), in the band accessible to pulsar timing arrays.

Testing GR and black hole physics. The principal characteristic of GR is the weakness of the coupling between the geometry of space-time and the dynamics of its content. Thus, it follows that the GW which we may detect are produced by phenomena occurring in *strong* gravitational fields, and imply strongly self-gravitating objects. Moreover, deviations of the waveform of the GW from GR predictions (as suggested e.g. by alternative theories of gravitation) can be used to infer constrains on beyond-GR theories and determine parameters such as the eventual mass of the graviton or the spin of the gravitational field.

What's more, the physics of black holes, the geometry of space-time in their vicinity and their intrinsic parameters such as spin and mass-radius relation can be attested by their gravitational signature in coalescences.

The data from the three first detections was used in [3] to put boundaries on deviations from GR, and it was found that with a 90% confidence level, the mass of the graviton is lower than $\sim 10^{-22}$ eV. Studies of the coalescence phase of the black holes have not shown significant variance from GR.

The GW spectrum. To sum up the expected GW sources and typical bands associated to these, figure 5 presents the GW spectrum, as well as the detectors likely to observe the corresponding bands.

2 Principles of gravitational interferometry

Light has played a central role in all physical theories since the foundation of Special Relativity (SR) in 1905 by Albert Einstein. The velocity of light is experimentally the only scalar quantity any two observers agree on, and all measurements of physical quantities must fundamentally use this unique property of light. That is why measuring distances in SR implies exchanging photons, it is also why synchronism, space and time intervals are relative.

In a more complex context, light is a standard way of probing the curvature of space-time, because light follows null geodesics in curved space. Thus deriving the geometry of a region of

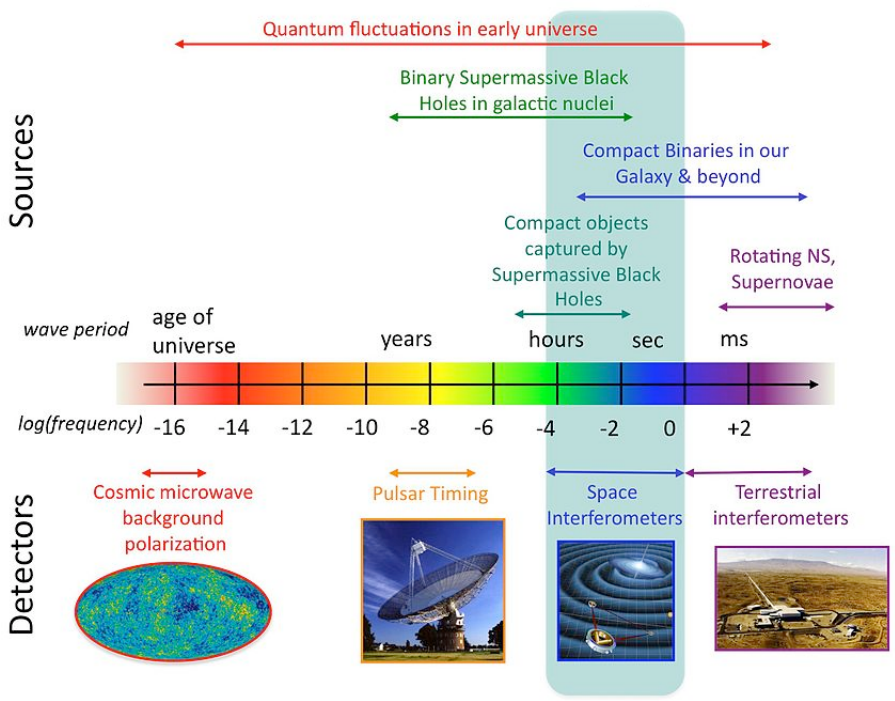

Figure 5: The GW spectrum and the GW detector network (Wikicommons).

space that has been traversed by light is theoretically straightforward if one knows the trajectory the light followed during its travel. Thus, the curving of space-time by the passing of a GW must be detectable with a light probing instrument, i.e. an optical setup. This is exactly the scope of gravitational interferometry and we will describe here the basic interferometry setup and its limitations before introducing the setup of Advanced Virgo.

2.1 Signal and noise

Detection is the competition between a physical signal and noise at the output of an instrument. Any noise is a centered stochastic process, meaning that it can be described by random variables which have a null mean value and a certain variance. Improving a detection system is modifying the detector in order to reduce as much as possible the variances of all these random variables, so that *on average*, the noise is closest to zero and any possible signal is easier to discriminate from the noise.

These variances may be described by the *spectral density* of the stochastic process. This is a function of a certain frequency and defined for a stochastic time-series $x(t)$ by:

$$S_x(\Omega) \;=\; \lim_{T\to\infty} \frac{1}{T} \mathrm{E}\left[\left|\int_0^T e^{-i\Omega t} x(t) dt\right|^2\right]$$

One may interpret this as the *variance of the random variable given by the Fourier transform at frequency* Ω of the signal. For every frequency Ω, calculating the variance of the Fourier transform coefficients of $x(t)$ after many runs yields $S_x(\Omega)$. A more handy function is the *root* of the spectral density, given by:

$$S_x^{1/2}(\Omega) \;=\; \sqrt{S_x(\Omega)}$$

For every Ω, $S_x^{1/2}(\Omega)$ is the standard deviation of the distribution of the Fourier coefficients obtained after many measurements of the signal.

The expectation value of noise is zero, thus the variable to act on to diminish the noise is its variance, i.e. its spectral density. Now, when a detector produces a channel containing a physical signal and some noise, the game is to improve the detector so that the spectral density of the noise is as small as possible (at all frequencies) so that the probability that the noise is effectively zero is large and that the probability that the signal is larger than the noise is large. Thus, in order to evaluate if a signal is measurable, the spectral density of the channel with the signal has to be larger than the spectral density of the noise of the instrument, also called the *sensitivity curve*.

The *sensitivity curve* of the instrument is the spectral density of the noise of the instrument. Of course to measure this sensitivity curve would theoretically take in infinite amount of time because to obtain the Fourier coefficients exactly one has to integrate over an infinite time. In practice, the sensitivity curve is measured over a short period of time.

Figure 6 represents the target sensitivity curve for Advanced Virgo as reported in the technical design report [12].

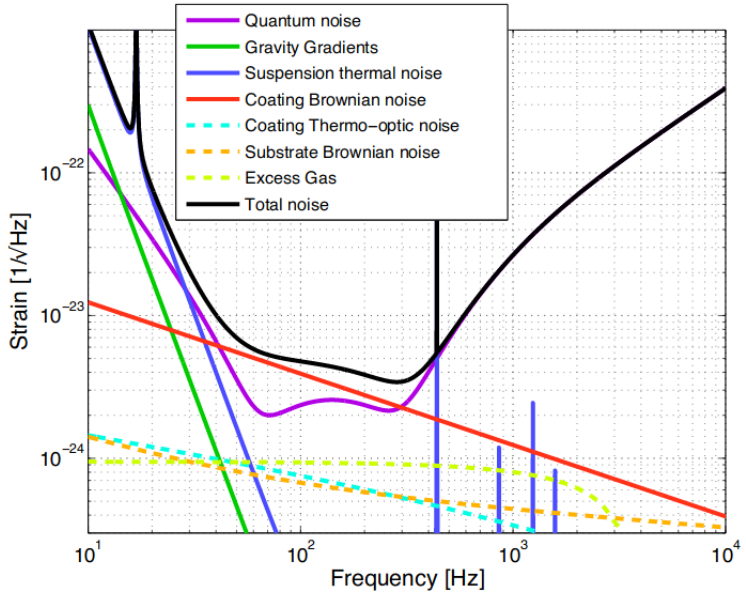

Figure 6: The target sensitivity curve for Advanced Virgo (from [12]). This curve is in the configuration where the signal recycling setup is optimized for binary neutron star merger. One can evaluate the contributions of every distinct noise.

2.2 The simple shot noise limited Michelson interferometer.

We will know describe a simple prototype of gravitational interferometer to illustrate these concepts.

Shot noise and power detection. Let us imagine a photodiode placed in front of a beam which has a (macroscopic) mean power of P_0. This instrument depends on quantum phenomena such as photoelectric emission and thus the effective number of photons detected during a given slice of time Δt is a discrete stochastic process N. We may even say that this *waiting and counting* process is described by a Poisson distribution of mean m. The probability for n photons to be detected during each Δt slice is:

$$p_n = e^{-m}\frac{m^n}{n!}$$

Moving to the detected power as given by:

$$P = \frac{Nh_p\nu}{\Delta t}$$

where h_p is Planck's constant and $\nu/2\pi$ is the frequency of the beam, we conclude that the variance of P is:

$$\begin{aligned} V[P] &= V[N]\frac{h_p^2\nu^2}{\Delta t^2} \\ &= E[N]\frac{h_p^2\nu^2}{\Delta t^2} \\ &= \frac{P_0\Delta t}{h_p\nu}\frac{h_p^2\nu^2}{\Delta t^2} \\ &= \frac{P_0 h_p\nu}{\Delta t} \end{aligned}$$

where we have used that $E[N] = V[N]$ for a Poisson process. We have thus obtained the variance for a *discrete* measurement of the power output of a beam. It can be shown by explicitly calculating the integral in the definition of the spectral density and letting $\Delta t \to 0$ that this expression may be generalized to the case of a continuous measurement of the power, i.e. a stochastic time-series $P(t)$. Namely, the spectral density of the output power of a photodiode is:

$$S_P(\Omega) = 2P_0 h_p\nu \tag{1}$$

This is *shot noise*, also called *quantum noise* because of its origin. It signifies that one cannot predict the power of the beam incident on the photodiode because the quantum rules of probability limit the actual number of photons detected by the diode. It is a fundamental noise of all detectors.

Notice that this is *white noise* because the density is constant. Our conclusion is that if we make a large number of measurement runs, we will obtain a sample of P's, which will all have a (time) mean of P_0. If we then calculate for each sample the Fourier coefficient corresponding to a given frequency Ω, then the distribution of the coefficients we obtain will have a mean value of 0, and a standard deviation of $\sqrt{2P_0 h_p\nu}$. This variance does not depend on Ω.

In turn, if someone increases the power of the laser for a short time then resets the power to its usual value, that will produce a temporary increase in the output power. In that *particular* measurement run, the spectral density of the signal will be modified around the frequencies relevant to the actual action of the person who fiddled with the laser amplifier. Only, the new shape of the spectral density could well have been produced by the shot noise, because the power output is a stochastic process and the value assumed by the corresponding Fourier coefficients may well have been abnormally high in *that particular* measurement. Thus, we may say for example with a certain ratio SNR: in that particular run, the Fourier coefficients were SNR times larger than the standard deviation of the shot noise, thus it is highly unlikely that they were produced by shot noise, thus it is highly likely that someone fiddled with the amplifier, and we have detected someone in the laser lab with a signal to noise ratio of SNR.

The Michelson interferometer. The simplest setup one may conceive as a gravitational interferometer is a Michel interferometer setup. This layout is depicted in figure 7. $M1$ and $M2$ are mirror which we will consider perfectly reflecting for the sake of simplicity. BS is an ideal and balanced beam splitter and the signal is read of the output of the photodiode PD. a and b denote the lengths of the two arms of the interferometer.

For this discussion, we will suppose that the light is polarized in a direction orthogonal to the plane of the interferometer. As the beam (of wave number k) is split on the beam splitter, half on the signal is reflected on $M1$ and half on $M2$, then recombined on the beam splitter and the amplitude on output of the beam splitter is:

$$A_{out} = \frac{1}{2}A_{in}(e^{2ika} + e^{2ikb})$$

The corresponding power is:

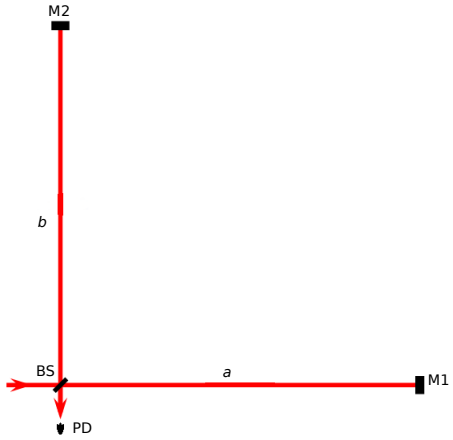

Figure 7: The simple Michelson gravitational interferometer. a and b: lengths of the North and West arms.

$$P \;=\; |A_{out}|^2 \;=\; \frac{P_0}{2}[1+\cos(2k(a-b))]$$

where we have noted by P_0 the input power.

Now suppose that the length of the North arm can vary and this variation is the goal of our measurement. Writing by $x(t)$ this variation and supposing that its time variation is slow compared to the circulation time of the light in the interferometer, we can derive the output power as:

$$P(t) \;=\; P_{DC} + \Delta P(t)$$

where P_{DC} appears as the output power of the interferometer in absence of the variation of an arm length and is given by:

$$P_{DC} \;=\; \frac{P_0}{2}[1+\cos(2k(a_0-b))]$$

and $\Delta P(t)$ is the power signal due to the variation of the arm length. It is (at first order supposing $x(t) \ll \lambda$):

$$\Delta P(t) \;=\; -P_0 k \sin(2k(a_0-b))x(t)$$

Notice here that one may tune the lengths a_0 and b in order for the interferences of the static interferometer to be:

- constructive, when $2k(a_0-b) \equiv 0[2\pi]$ and consequently $P_{DC} \;=\; P_0$. The interferometer is then said to be *tuned to a bright fringe*
- destructive, when $2k(a_0-b) \equiv \pi[2\pi]$ and consequently $P_{DC} \;=\; 0$. The interferometer is then said to be *tuned to a dark fringe*.

To maximize the signal to noise (SNR) ratio in the case of a signal, a dark-fringe-tuned setup is preferable. Nonetheless, such interferometers do not allow to distinguish x and $-x$ because of the symmetry of $P(t)$ under this substitution is the case where $2k(a_0-b) \;=\; (2n+1)\pi$. For this reason, the Virgo interferometer is not quite tuned to a dark fringe, but not far.

Detection limit for the shot noise Michelson interferometer. If the signal $\Delta P(t)$ is not null, then we may measure the corresponding variation of the arm length. Writing $\beta = 2k(a_0 - b)$, the signal is:

$$\Delta P(t) = P_0 k \sin(\beta) x(t)$$

As we have described in section 2.1, we must compare the spectral density of this signal to that of the noise in order to determine if the signal is distinguishable from the noise. We will consider here only the shot noise (or quantum noise) of the photodiodes as expressed in equation (1).

The spectral density of ΔP is:

$$S_{\Delta P}(\Omega) = P_0^2 \sin(\beta)^2 k^2 S_x(\Omega)$$

Now the effect of a GW on a object is the vary its dimensions, thus we may for example write $x(t) = Lh(t)$, L being the static length of the arm and $h(t)$ the gravitational wave signal. And thus:

$$S_{\Delta P}(\Omega) = P_0^2 \sin(\beta)^2 k^2 L^2 S_h(\Omega)$$

The shot noise here is that corresponding to the DC output and accordingly with 1 is thus:

$$S_{SN}(\Omega) = 2P_{DC} h_p \nu = h_p \nu P_0 (1 + \cos(\beta))$$

The signal to noise ratio for each frequency Ω is thus:

$$SNR(\Omega) = \frac{2\pi}{\sqrt{h_p c}} \frac{\sin(\beta)}{\sqrt{1+\cos(\beta)}} \sqrt{\frac{P_0 L^2}{\lambda}} S_h^{1/2}(\Omega)$$

Note the optimization degree of freedom in $\sin(\beta)/\sqrt{1+\cos(\beta)}$, which we will suppose equal to 1 here ($\beta = \pi/2$, half way between dark fringe and bright fringe).

Conversely, one may wonder what is the minimal signal one can pick up on this instrument. The minimal signal is such that the SNR is equal to one on every frequency of the band of the instrument. This signal has a minimal spectral range of:

$$S_{\min}^{1/2}(\Omega) = \frac{\sqrt{h_p c}}{2\pi} \sqrt{\frac{\lambda}{P_0 L^2}} \tag{2}$$

In the case of the Virgo interferometer, where $P_0 \sim 20$ W, $\lambda \sim 1064$ nm and $L \sim 3$ km, the minimal signal must have a root spectral density of at least $\sim 0.5 \times 10^{-21}\ 1/\sqrt{\text{Hz}}$.

As we can see by comparing with the typical signals reported in section 1.3 figure 3, another 2 orders of magnitude of precision are needed to detect black hole coalescences or neutron star mergers. We will detail three of the main improvements of the setup which allow the Advanced Virgo to reach the required sensitivity.

2.3 Introduction to the optical layout of Advanced Virgo

The sensitivity of the simple shot noise limited Michelson interferometer is constrained by two main parameters as explicit in equation (2): the length L of the arms, and the power P_0 incident on the beam splitter. The larger these two parameters, the smaller the $\frac{1}{\sqrt{P_0 L^2}}$ factor in the minimal detected signal. These parameters may be effectively increased by *power recycling* and *Fabry-Perot resonance* features to be implemented in Advanced Virgo, and the sensitivity can be further increased by a *signal recycling* setup. We will now briefly describe these setups.

Figure 8 is a schematic of the layout of a power-recycled Michelson interferometer with Fabry-Perot cavities as arms. This is the skeleton layout of the Advanced Virgo and we will know advocate this layout.

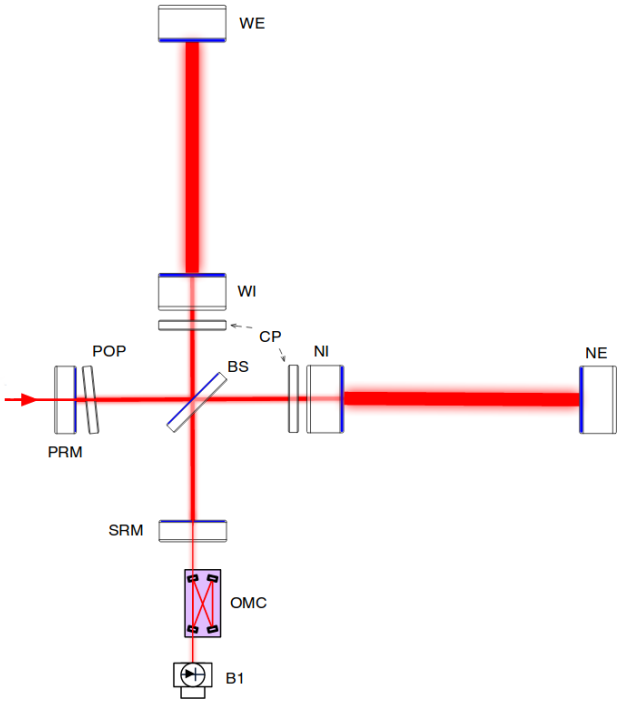

Figure 8: The doubly-recycled Michelson-Fabry-Perot interferometer of Advanced Virgo (adapted from [12]). WE-WI and NE-NI: mirrors of Fabry-Perot cavities (west and north), PRM and SRM: power and signal recycling mirrors, CP: compensation plates, to compensate for thermal effects on WI and NI.

Fabry-Perot cavity resonances. A Fabry-Perot cavity is composed of two facing mirrors $M1$ and $M2$ at a distance of L from each other (see figure 9). This setup is resonant for a certain discrete set of frequencies, all separated by the so-called *free spectral range*:

$$FSR = \frac{c}{2L} \tag{3}$$

The quality of the resonance (the width of the resonance peaks) can be measured by the *finesse* parameter:

$$F = \frac{\pi\sqrt{r}}{1-r}$$

where r denotes the reflectivity of the $M1$ mirror, we have supposed $M2$ perfectly reflective and no losses inside the cavity.

Indeed, the width of the resonance peak is:

$$\delta\nu = \frac{FSR}{F}$$

and we thus understand that the quality of the resonance is measured by F.

Let ν_0 denote a resonant frequency of the cavity, ν the frequency of a input beam and $f = \frac{\nu-\nu_0}{\delta\nu}$. Then the complex reflectivity of the cavity (i.e. B/A) is:

$$R(f) = -\frac{1-\sigma+2if}{1-2if}$$

where $\sigma = pF/\pi$ and p is the total loss of the cavity.

Notice that $R(0)$ is a real number, signifying that if the input beam and the cavity are matched, there is no phase shift upon reflection on the cavity.

Now, if in the course of the passing of a GW the length of the cavity is modified by a scale h, the resonant frequencies of the cavity will also shift, accordingly with equation (3). The input beam will thus no longer be matched to the cavity and $R(f)$ will pick up a non-null phase. Thus the reflected beam will be phase-shifted with respect to the input beam. This phase shift is exactly analogous to the $e^{2ik\delta L}$ phase shift of the basic Michelson corresponding to the path of the light in the arms.

This phase shift is:

$$\Delta\Phi \ = \ \frac{4}{\pi} iFk\delta L$$

Thus, the Fabry-Perot cavities replace the $2\delta L$ optical path of the simple Michelson interferometer by a $\frac{4}{\pi}F\delta L$ path in terms of phase shift. Virtually, the interferometer's arms are lengthened by a factor $\frac{2}{\pi}F$, and the sensitivity is increased by a factor of the same order of magnitude. In the case of Advanced Virgo, the finesse objective is 443 according to [12].

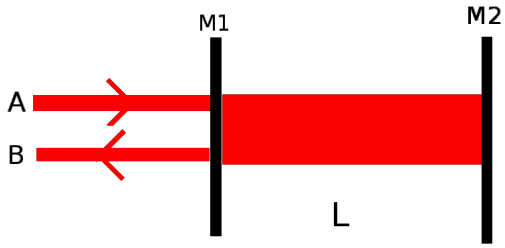

Figure 9: The Fabry-Perot cavity, one is interested in the phase shift between in in coming beam A and the reflected beam B.

Power recycling. Power recycling consists in placing a mirror at the input of the Michelson interferometer. In this fashion, the power which is transmitted by the beam splitter away from the north arm is not lost to the interferometer, but reflected back inside. The overall power of the incident beam is thus increased and the so is the sensitivity, accordingly with the discussion of section 2.2.

Signal recycling. Another strategy to increase the sensitivity is the signal recycling setup. By adding a resonant cavity materialized by a mirror at the output of the Michelson interferometer. By tuning the characteristics of this cavity, one may change the shape of the sensitivity curve in order to insist on a certain band, and thus adapt the instrument to a certain source.

3 The optics of gravitational interferometry

In this section, we will describe the particularities of gravitational observatories in terms of Gaussian optics simulation, then overview the available tools and their limitations[1] as a motivation for a new software. This will lead us to the requirements for the new Gaussian beam simulation tool and the description of `theia` in the next section.

3.1 3D setups and astigmatic Gaussian beams

Orthogonal Gaussian beams. Gaussian beams are mono-chromatic directionally-localized light beams. They are represented by solutions to the electromagnetic wave equation, under the

[1] Please note that many of the softwares we will mention here are excellent tools and our inspiration in making a new tool was broadly found by reviewing these codes. We will underline their limitations for the sake of argumentation and in order to introduce our work, but one must not be misled by our words.

paraxial approximation: the non-oscillating component of the electromagnetic field amplitude does not vary rapidly along the beam's direction, with respect to the oscillating component. In other words, the electromagnetic field amplitude is decomposed in:

$$F(x,y,z,t) \;=\; e^{i(\omega t - kz)}E(x,y,z)$$

where (x,y,z) is a orthonormal coordinate set such that z is the direction of propagation of the beam, and ω and k are the angular frequency and vector number of the oscillating component $e^{i(\omega t-kz)}$. The paraxial approximation claims that:

$$\frac{\partial E}{\partial z} \ll kE$$

Solving the wave equation with velocity $c = \omega/k$ yields the so-called *eikonal* equation on E:

$$(\Delta_{x,y} + 2ik\partial_z)E(x,y,z) \;=\; 0 \tag{4}$$

in which $\Delta_{x,y}$ is the Laplacian operator in the transverse plane.

This equation is known to generate discrete families of solutions (of *Transverse Electromagnetic modes*, TEM), which form bases for developing any solution to this equation and thus approximate fits for real Gaussian beams, e.g. produced by lasing devices.

The fundamental mode to consider, as it generally contains the largest part of the energy of the total beam, is the TEM_{00} mode. In its general form, it is in some othogonal (x,y,z) coordinates (see [22] for a derivation):

$$E(x,y,z) \;=\; E_0(z)\exp\left[i\eta(z) - i\frac{k}{2}\left(\frac{x^2}{q_x(z)} + \frac{y^2}{q_y(z)}\right)\right] \tag{5}$$

in which q_x and q_y are complex numbers which contain explicit physical information as we will see shortly. There exist four integration constants $z_x^0, z_y^0, z_x^R, z_y^R$ such that:

$$q_{x,y}(z) \;=\; (z - z_{x,y}^0) + iz_{x,y}^R$$

With these definitions, we have:

$$E_0(z) \propto \left(\mathrm{Im}\left(\frac{1}{q_x(z)}\right)\mathrm{Im}\left(\frac{1}{q_y(z)}\right)\right)^{1/4}$$

$\eta(z)$ is the so-called *Gouy* phase:

$$\eta(z) \;=\; \frac{1}{2}\left[\arctan\left(\frac{\mathrm{Im}(q_x)}{\mathrm{Im}(q_x)}\right) + \arctan\left(\frac{\mathrm{Im}(q_y)}{\mathrm{Im}(q_y)}\right)\right]$$

Let us suppose that $z_x^0 = z_y^0$ and $z_x^R = z_y^R$.

Now, the directions pointed to by x and y axis are seen as principal directions of the beam (they are in the transverse plane). Indeed, if we make a section of the beam at an abscissa Z, then the curves of constant amplitude $|E(x,y,Z)|$ or phase $\arg(E(x,y,Z))$ are ellipses in the resulting plane. More, for each constant amplitude ellipse, there exists one constant phase ellipse, and these two ellipses have the *same* semi-axis directions, which are directions x and y. If we pick the ellipse of the section at Z of amplitude equal to $1/e^2$ of the total beam power, and then vary Z, this ellipse draws an elliptical hyperboloid in space. That hyperboloid has a *waist* made of an ellipse of semi-axis $w_x = \sqrt{\frac{\lambda z_x^R}{\pi}}$ and $w_y = \sqrt{\frac{\lambda z_y^R}{\pi}}$ (always in the x and y directions of course). This is the interpretation of the *Rayleigh* ranges $z_{x,y}^R$. This waist is positioned at an abscissa $z_x^0 = z_y^0$ along the direction of the beam. This interpretation is summed up in figure 10.

Note that Gaussian beams are characterized by a relationship between their divergence and their waist: their product is constant and thus a strongly diverging beam has a small waist and conversely[2].

[2] In the case of a non-diverging beam, i.e. a plane wave ($E(x,y,z) = 1$), the optics reduce to geometrical optics.

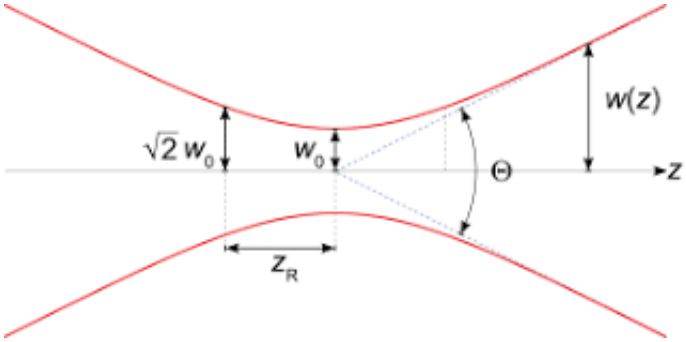

Figure 10: A section of the beam in the xz plane. The red hyperbola is the surface of amplitude equal to $1/e^2$ of the total power. An illustration of the Rayleigh range z_R is also given. Its waist is $w_0 = w_x$. The divergence of the beam Θ is $2\lambda/\pi w_0$. A similar hyperbola is reproduced in a section on yz, but with a different waist. In orthogonal beams, the two waist are at the same abscissa and the ellipses are circles (Wikicommons).

Astigmatic beams. The beams we have just described are *orthogonal* beams and verify that the two waists are at the same abscissa $z_x^0 = z_y^0$ and the ellipses are circles $z_x^R = z_y^R$. In the general case and experimentally, beams are seldom orthogonal, they are *astigmatic*, i.e. $z_x^0 \neq z_y^0$ and $z_x^R \neq z_y^R$. These beams may be described more compactly in their principal coordinate system:

$$E(x,y,z) = E_0(z)\exp\left[i\eta(z) - i\frac{k}{2}{}^t r Q(z) r\right]$$

in which $r = (x,y)$ is the transverse coordinate vector and

$$Q(z) = \begin{pmatrix} \frac{1}{q_x(z)} & 0 \\ 0 & \frac{1}{q_y(z)} \end{pmatrix}$$

is a diagonal matrix, named the *curvature tensor*.

This form is explicit on the second order nature of the phase (thus the ellipses and hyperbolae as constant amplitude and phase surfaces). Under a rotation around the z axis into new coordinates r', the amplitude becomes:

$$E(x,y,z) = E_0(z)\exp\left[i\eta(z) - i\frac{k}{2}{}^t r' Q'(z) r'\right]$$

In which Q' is the conjugation of Q by the rotation matrix R: $Q' = RQR^{-1}$.

Explicitly:

$$Q'(z) = \begin{pmatrix} \frac{\cos^2\theta}{q_x(z)} + \frac{\sin^2\theta}{q_y(z)} & \frac{1}{2}\sin 2\theta\left(\frac{1}{q_x(z)} - \frac{1}{q_y(z)}\right) \\ \frac{1}{2}\sin 2\theta\left(\frac{1}{q_x(z)} - \frac{1}{q_y(z)}\right) & \frac{\sin^2\theta}{q_x(z)} + \frac{\cos^2\theta}{q_y(z)} \end{pmatrix}$$

for some real angle θ.

The fundamental property of *astigmatic* beams are that there exists a basis in which the curvature tensor Q is diagonal, i.e. a set of coordinates in which the phase reduces to the familiar form $\exp(-i\frac{k}{2}(x^2/q_x(z) + y^2/q_y(z)))$ of equation (5).

In fact, this property defines astigmatic beams and it is conserved all along the propagation of the beam as along as in every interaction with an optical component, one at least of the principal directions of the beam is parallel to the interface surface. In particular, this property is conserved by interaction on cylindrical surfaces when the axis of the cylinder is parallel to one of the directions of the incoming beam, by interaction on plane surfaces, etc. It is *not* preserved by interaction on spherical or parabolic surfaces.

As derived above, the ellipse of constant phase and of constant amplitude of astigmatic beam have the same principal directions.

General astigmatic beams. Upon interaction with spherical surfaces, astigmatic beams lose this property: their constant phase and constant amplitude surfaces no longer have the same principal axis, as it can be shown experimentally with a photodiode (which measures amplitude) and a phase camera (which measures phase).

In this case, *there does not exist* a set of orthogonal coordinates in which Q is diagonal. These are the *general astigmatic beams* and are common in 3D setups comprising spherical surfaces.

In fact, these beams are correctly described by multiplying the curvature tensor as an astigmatic beam by a rotation matrix which has a *complex* angle. These are the most general solutions to the eikonal equation (4). This angle is conserved by the propagation in free space and is interpreted in the following way: its real part $\mathrm{Re}\theta$ provides the rotation to find the principal directions of the power ellipse, and its imaginary part $\mathrm{Im}\theta$ provides the angle between the power and phase ellipses.

Thus, to describe general astigmatic beams, it suffices to provide two principal vectors and a matrix of the form

$$Q'(z) \;=\; \begin{pmatrix} \frac{\cos^2\theta}{q_x(z)} + \frac{\sin^2\theta}{q_y(z)} & \frac{1}{2}\sin 2\theta\left(\frac{1}{q_x(z)} - \frac{1}{q_y(z)}\right) \\ \frac{1}{2}\sin 2\theta\left(\frac{1}{q_x(z)} - \frac{1}{q_y(z)}\right) & \frac{\sin^2\theta}{q_x(z)} + \frac{\cos^2\theta}{q_y(z)} \end{pmatrix}$$

with θ a complex angle.

Transformation of general astigmatic Gaussian beams. There are mainly three ways a Gaussian beam can transform. In each case we will detail the laws which provide the curvature tensors of the beam resulting from the interaction as a function of that of the incident beam[3].

1. Under free propagation, one seeks to know the curvature tensor after a distance Δz, $Q(z_0 + \Delta z)$ as a function of the tensor at z_0. This is given by:

$$Q(z_0 + \Delta z) \;=\; (I + \Delta z Q(z_0))^{-1} Q(z_0)$$

   where I is the identity matrix in 2 dimensions.

2. Under a reflection or a refraction on a spherical surface, a phase matching method relying on the fact that the phase is continuous at the interface leads to simple laws which are extensively detailed in [21]. These laws computationally reduce to matrix multiplications concerning the incoming curvature tensor and the matrices representing the curvature of the surface.

The physical interpretation of general astigmatic beams. Starting from a curvature tensor to deduce physical properties such as waists and Rayleigh ranges is straightforward in the case of astigmatic beams, because it suffices to diagonalize the tensor and extract the real and imaginary parts of the diagonal terms.

In the case of the general stigmatic beam, the process is not nearly as clear mainly because there *is no* clear physical interpretation of the coefficients of the tensor in terms of Rayleigh ranges, waists, etc. Nonetheless, θ and $q_{x,y}$ can be extracted from the curvature tensor and we interpret the beam by regarding it as if it were the astigmatic beam characterized by $q_{x,y}$ and $\mathrm{Re}(\theta)$. Indeed, this astigmatic beam is the one which best interpolates the real (general astigmatic) beam and thus is fit for interpretation.

3.2 The optics context of gravitational observatories and requirements for new software

The context of optics in gravitational observatories are peculiar and impose requirements on the tools used in simulation.

[3] For a full derivation of these results and their explicit statement, see [21, 22].

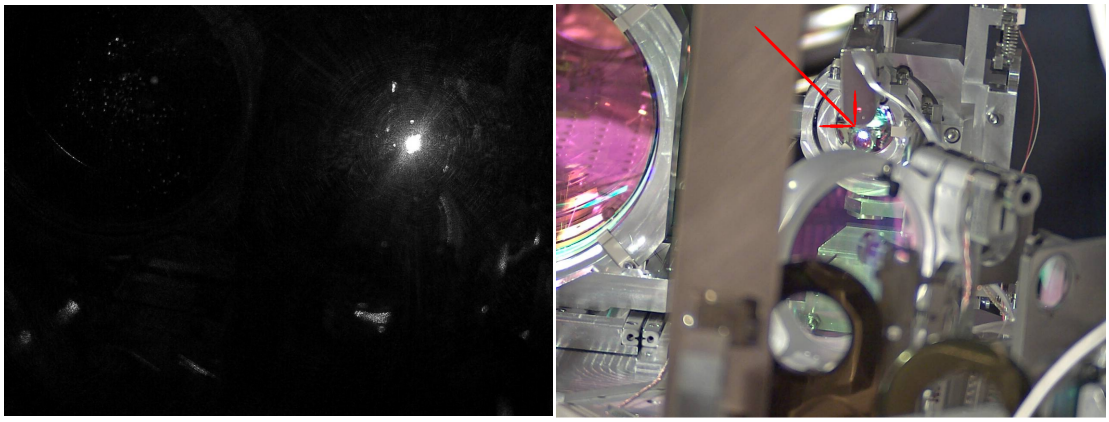

Figure 11: A ghost beam spotted in the detection bench as the interferometer is locked (Virgo logbook entry 38150, courtesy of A. Allocca and A. Chiummo). Left: lights off, one spots this stray light in the optical setup, right: the same spot (red arrow) with the lights on, one realizes the spot is on a mirror behind the camera, we see the image of this mirror by reflection on the mirror at the right of the image.

Scattered light and ghost beam hunting. From the power recycling mirror onwards in the interferometer, an estimated 81 W of the incident 125 W beam on the power recycling mirror (65% of the light) is lost by scattering. That is, light which is found outside of its intended path because of imperfections of the optical setup and of its components, of second order effects of the light on materials or of unintended optical effects in the interferometer. This light may be reflected off a low-reflectivity surface, caused by some beam clipping and thus diffraction on an optical component or can accidentally interfere with the main beam of the setup. As a consequence, this light produces unintended signals in detectors, decreasing the overall sensitivity, and may also produce thermal deformation effects on other components by heating, and reflect or diffract on mechanical components, leading to even more noise on detectors and jitter on the infrastructure of the interferometer.

Going inside the interferometer's chambers or using the numerous cameras installed along the setup allows to spot these *ghost* beams (as in figure 11) and try to evacuate them from the setup by inserting light absorbing media such as baffles or directly acting on the setup at hand, which is a far more delicate operation. Only, the spot appearing on the wall of the tunnel or tower harboring the setup may be – and often is – the result of a complex path in the optical setup. A primary ghost beam (produced by either of the mechanisms detailed in this last paragraph) may reflect, diffract or be refracted many times on the components or walls before resulting in the spot seen by the observer. Thus, it is necessary to able to *reverse trace* a beam produced by a simulation to the original beam, in case it is a ghost beam.

If one could find a ghost beam by using a camera, identify the corresponding beam in a simulation and retrace the beam tree up to the original unintended beam, then the task of ghost beam hunting would be more readily accomplished. This is one of he scopes of our new software, `theia`.

Whatever the shape of the output of the new software, it must allow easy navigation among the generations of beams, in order to hunt ghost beams up to their original progenitors and take action rapidly.

Optical setups at a glance. The Virgo interferometer is a kilometer-scaled optical setup. Thus, it is important to be able to have a global view of the instrument easily, because the health of the setup and global checks such as the existence of beams all the way through the setup, the irrigation of each sub-system with light, etc. must be done quickly, before going into the details of the Gaussian parameters of the beams.

This global view is not provided by a list of numbers concerning beams, nor by a single sheet of schematics overseeing the entire setup, but only by a dynamical software which allows to navigate

the setup in three dimensions, zoom in and out of sub-systems and perform translations and rotations of the view. These extremely helpful features are provided by standard Computer Assisted Design (CAD software), well known to engineers for there ease of use in solid mechanics projects.

Thus, the choice was made to render in 3D the results of the simulation of the new software, by writing a CAD file holding the relevant beams and optics, to be read by a CAD software in order to navigate easily among the generated beams and the optical setup.

From the laboratory to the interferometer. The optical activity of gravitational interferometers is held in two places: in the optics laboratory, where the design and testing of sub-systems is led, and on the interferometric instrument site itself. Thus it is a requirement that the texts file for input and output of `theia` be portable. By this we mean that an output file is concise and holds the necessary information to be printed out and taken to the interferometer for comparison with experimental data, and that an input file is flexible, can make reference to the optical components by literal references and labels, and not only positions in 3D. Globally, `theia` input and output files are meant to use a high-level language, which make sense at a glance in an experimental context.

3D beams exactitude of beam direction and alignment. Of course, contexts such as gravitational interferometers require precise simulations. The orders of magnitude of the phenomena occurring in gravitational interferometers (as presented in section 1.3, figure 3) are an indication of the precision which is to be found in the optical setups in terms of beam direction, alignment and Gaussian parameters.

Thus, it is important that a minimum of approximations be assumed and that the input by the user be as arbitrarily precise as the user intends. The approximations supposed and the algorithm used by `theia` are reviewed in section 4.4 of this report.

Thermal and mechanical constraints and effective optics. In gravitational observatories, optical setups are placed in an environment which is prone to thermal and mechanical constrains. The shape and thus the optical properties of components adapt accordingly to the mechanical strain on a bench or to the thermal conditions induced by the absorption of light by optical materials. These effects are intense because the orders of magnitude of the powers at hand are large (650 kW of power in the arms, 4.9 kW incident on the beam-splitter) and because one needs to conserve the optical precision in the instrument.

It may thus be necessary to resort to *effective optics*, in other words to find the optical component which is equivalent to the observed effect in order to compensate the effect by inserting a new component such as a lens or a mirror. Thus, it is necessary to provide a means of *dynamically* change the simulation input and optimize the setup by varying such and such parameter until one is satisfied, without the hassle of rewriting a configuration file each time.

This is a part of *simulation scripting*, which gives the user full control on the flow of the simulation and the power to write his or her own algorithm to optimize such and such parameter of the setup. Examples of this procedure in the context of a thermal lensing effect and of optical design are given in the last section of this report.

`theia` helps to serve this particularity of gravitational optics by being modular at most. Indeed, being a stand-alone command line tool and also a complete Gaussian beam tracing library, it may fit the uses of straight-forward simulation of a setup by reading in a configuration file, but also the uses of scripting by being imported into custom scripts. In order to guarantee these features, `theia` is written in the vastly known and used Python language, as it is fit for scripting, common in the world of physics and portable. Care has also been taken in writing clear and commented sources, extensive documentation and tutorials.

3.3 Current solutions for simulation

The requirements `theia` attempts to fulfill are partly provided by existing tools. We will review the most common of these, and detail the inspiration which they provide in the development of `theia`.

`OptoCAD`. `OptCAD` ([23]) is vastly used in the gravitational interferometry community. It was written by Roland Schilling, a pionner of the power recycling setup ([6]).

`OptoCAD` allows for the simulation of astigmatic (not *general* astigmatic) Gaussian beams through a plane setup composed of optics the user specified surface by surface. Thus, a large palette of optical components is available, being limited only by the number of combinations of reflections and transmissions one can find. It supports interferences, cavity treatment and allows the user to control in what form the output of the simulation is supplied: a text file with selected Gaussian parameters for each beam, a Post Script (PS) schematic of the setup centered and framed as the user wishes, etc. `OptoCAD` also allows to stop a beam and restart it identically at another point in the setup, which is handy for emulating 3D setups, but is limited to *parallel* optical benches.

The main drawback of `OptoCAD` is that it does not take truly 3D setups into account, and its scripting capabilities are limited by the fact that it is written in Fortran and its sources are poorly organized and documented.

`gtrace`. `gtrace` ([24]) was developed by Yoichi Aso of the KAGRA collaboration. It is a very modular and powerful scripting library, written in Python. It accounts for astigmatic beams in a planar setup, and the optics may be mirrors or cavities. It does not calculate interferences *per se*, and does not provide a stand-alone tool for simulation. It provides PS viewing of the setup after simulation. The sources are clear and commented, which allows for ready scripting and automization.

`gtrace` was the single most influential inspiration for `theia`, especially for the tracing algorithm and the use of simulation orders and thresholds to insure termination.

`Zemax`. `Zemax` ([25]) is proprietary software. It does not allow scripting and its features are limited to what its developers permit. It allows sequential and non-sequential tracing, though these two modes poorly communicate, and simulates orthogonal beams. `Zemax` allows to keep a bank of optics to be picked from in future simulation, much like a text configuration file which can be kept and reused for further simulations.

4 `theia`: a new tool for gravitational observatories

In this section, we will be more explicit on the physics and algorithms behind `theia`.

4.1 The theia rationale

`theia` has been designed for flexible and practical operation. This why `theia` is not only a command line tool, but also a Python library aiming at scripting and written accordingly.

The `theia` command line tool has it its own right been designed with flexibility and pragmatism in mind. The `theia` input and output files were thought to allow high level features to insure ease of writing and reading by humans, to be printed out, brought to the optical bench and used as references to follow the evolution of the optical layout and its components, to be read as structured files containing figures one can readily compare to experimental data, etc. Finally, the goals of flexibility and pragmatism also lead to the conception of an extensive user environment, hosted at `http://theia.hopto.org`.

Aiming for flexibility also implies liberty for the user when it comes to input. The user can specify as much information as she or he wishes. From specifying zero parameters and using default values for all the arguments to using built-in values such as handy units, users have a large radius of action for their input.

With liberty must also come caution. If the user specifies geometrically inconsistent parameters – leading to self-intersecting surfaces for instance –, then warnings may be issued to standard output (unless specific command line flags are used) but the simulation will carry on almost unseemingly, and may lead to unexpected behavior.

4.2 The operation of theia

`theia` is a command line 3D Gaussian beam tracing program. During its operation, input beams and an optical setup are read from an input text file and these beams are traced and interact with optical components. Following the rules of geometrical and Gaussian optics, and according to some selection rules designed to insure the termination of the program, this process produces new beams, by reflection and transmission of the former beams on the surfaces of the optical components. This creation and selection process is repeated recursively in order to calculate all the beams produced by the input beams and their geometrical and Gaussian characteristics.

This operation results in the writing of a text file containing the information on the traced beams and a CAD file for 3D visualization.

4.3 Beams and optics

The physical objects a representation of which `theia` deals with are general astigmatic Gaussian beams, and optical components in 3D general positions and orientations. This section describes how these objects are seen by `theia`.

Gaussian beams. Gaussian beams are described by two set of parameters: geometrical parameters and Gaussian parameters.

1. The geometrical parameters are the 3D position of the origin of the beam, the unitary 3D vector directing the beam and finally the length of the beam, from its origin to its end point. On input, the position of the origin is given by three coordinates and the direction by two angles forming spherical coordinates. The length of the beam is initialized to 0 and updated once we know if and where the beam ends by interaction.

2. The Gaussian parameters are threefold: one complex matrix and two unitary vectors, as described in section 3.1. It is so because the general astigmatic beam, as it forms by repeated oblique incidences on optics, is described on one polarization direction by the following equation on the electrical field:

$$E(\vec{r},t) \;=\; \exp(i\eta(z) - i\frac{k}{2}{}^t(x,y)Q(z)(x,y))e^{i(\omega t - kz)}$$

   in which z is the coordinate of $\vec{r}$, (x,y) its coordinates in the plane transversal to the beam's direction, Q is the curvature tensor, and η accounts for all other phase accumulation (Gouy, etc.). [4]

Thus, to specify completely the state of the beam at a position z along the beam, one has to specify two vectors (the eigen directions) which span the transversal plane, and the matrix $Q(z)$ in the basis of these vectors. From Q, one can derive the waists and positions of these waists, Rayleigh ranges, etc.

In `theia`, to each beam are attached these two vectors and the value of Q *at the origin of the beam.*

Inputting Gaussian data. Inputting to the `.tia` file only allows for astigmatic beams. Thus it is asked to the user to specify the waists and positions of these waists, and the angle of rotation of the beam (in the clockwise sens looking down the beam) with respect to the beam which has as a first eigen direction the vector with the largest possible global Z coordinate (and which is of course orthogonal to the beam direction).

In other words, if the user specifies a direction $\vec{dir}$ and an angle of 0, then she or he is saying that the first semi-axis of the amplitude ellipse (in which the first input waist and waist distance are found) is that unitary u vector orthogonal to $\vec{dir}$, and which has the largest possible Z coordinate.

[4] Note that in the case where the beam is astigmatic (but *not* in the general astigmatic case), there exists a orthogonal basis of the transverse plane in which the Q matrix is diagonal and the expression of the electrical field is reduced to a more familiar form $\exp(-i\frac{k}{2}(x^2/q_x(z) + y^2/q_y(z)))$.

See figure 12 for an illustration. And the second semi-axis is the unitary v vector such that $(\vec{dir}, u, v)$ is a right-handed orthonormal basis.

What if $\vec{dir}$ is directed by $\pm e_Z$ and the "largest possible Z coordinate" condition makes no sens? Then u is $\pm e_X$ and v is $\pm e_Y$.

Now, if the angle `Alpha` is not 0, then the basis the user means is the rotation of the `Alpha = 0.` case by an angle `Alpha` around $\vec{dir}$.

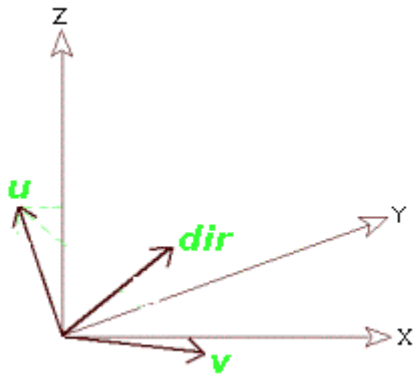

Figure 12: The `Alpha = 0` case. X, Y, Z is the global coordinate system, u is defined as being the vector orthogonal to the beam direction dir and having the largest global Z coordinate. v is chosen such that (dir, u, v) is a right-handed orthogonal basis. For a non-zero `Alpha` case, rotate u and v by `Alpha` around dir.

Optical components. Available optics are semi-reflective mirrors, beam-splitters, thin lenses (defined by their focal length and diameter), thick lenses (thickness on axis, refractive index, curvatures and diameter), mirrors and beam-dumps (which stop light). Optical components all have cylindrical symmetry, except for mirrors which may have a wedged face. The labeled "HR" surface is the principal surface, where beams are meant to be reflected of transmitted. In the case of mirrors it is the non-wedged surface.

Since mirrors can be wedged and do not have cylindrical symmetry, it is necessary to specify an angle to describe the position of the wedge in space. This is done in a similar fashion than in the beam case. If this angle (also called `Alpha` is 0, then the point of the AR (wedged face) which is not affected by the wedging (it is the point on the rim of the original cylinder the AR was wedged from) has the largest global Z component. Similarly as for beams, if the "maximum Z" condition makes no sense because the HR normal is $+e_Z$ (resp. $-e_Z$), then this reference point has largest (resp. smallest) X coordinate.

If `Alpha` is not 0, then this reference is situated at the image of the `Alpha = 0` reference point by the rotation of `Alpha` around the normal (outpointing) vector of the HR surface. See figure 13 for an illustration.

4.4 Algorithm and approximations

As previously described in section 4.2, `theia` traces beams by interaction of the input beams with the optics, recursively. Here are the rules to calculate the beams.

Physical rules. The laws of refraction and reflection are applied to calculate the directions of the new beams, as well as the origin Q matrix (and the base vectors to express it) of the new beams. The calculation of the Q matrix follows the phase matching method as detailed in section 3.1. Total reflection is also taken into account, and the powers of the new beams are calculated according to the reflectance and transmittance of the surface.

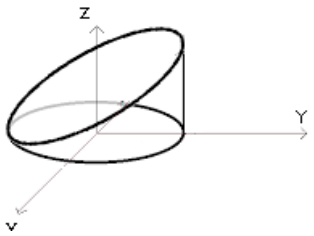

Figure 13: A mirror. Its center of HR is (0, 0, 0) and its normal to HR is $-e_Z$. Thus the reference point is (–1, 0, 0). Thus we can say that this is a thickness = 0, positive wedged mirror with `Alpha = 225 °` (angle between the reference point and the point of the rim of the original cylinder which touches the AR face). Note that we could have also said a thickness = 1, *negatively* wedged mirror with `Alpha = 45 °`.

This rule introduces the approximation that the radius of curvature of the beam must be much smaller than the radii of curvature of the optics at hand. Apart from this, there are no other approximations (nor for the geometrical optics calculations to determine the direction of the new beams, nor for the exact point of origin of the new beams on the curved surfaces[5]).

Computational rules. In order for the program to terminate, some computational rules have been introduced. Each simulation is led with an *order* and a *threshold*:

1. Each initial beam is created with a *strayness order* of 0. Any beam reflected by a mirror AR face, transmitted by a mirror HR face, or reflected by any face of a lens has the order of its parent beam, plus one. Beams with an order larger than the simulation order are excluded from the following calculation step and their children are not determined. More generally, each surface of an optic has a certain action on the order of beams, depending on the nature (reflected or transmitted) of the beam and of the optic. For example, the surfaces of beam-splitters do not increase the order of beams, whereas all surfaces of lenses increase the order of reflected beams by 1, and those of transmitted beams by 0. See table 2 or the *Quick Reference* document for a list of the actions of optics on beams.
2. The power of children beams are determined with the powers of the parent beams and the reflectance and transmittance of the surface. Similarly, beams with powers smaller than the simulation threshold are excluded from the following calculation step and their children are not determined.

Optic	**Action of ... HR on reflected**	**HR on transmitted**	**AR on reflected**	**AR on transmitted**
Mirror	+0	+1	+1	+0
Thick or thin lens	+1	+0	+0	+1
Beam-splitter	+0	+0	+0	+0
Special surface	User defined (see 4.1)			

Table 2: The actions of surfaces of optical components on the strayness orders of beams

4.5 Schedule of `theia`

In order to give a time scale to the development of `theia`, a schedule can be found in table 3.

[5] We are of course limited by the precision of floating pint numbers on the underlying machine.

Version	Date	Features
0.0.1	*May 10*	mirrors, tracing engine
0.1.0	*June 9*	lenses, beam dumps, standard input and output text files, warning and information outputs
0.1.1	*July 1*	ghost (inactive) surfaces, low-level 3D rendering
0.1.2	*July 24*	high-level graphics, clipping and anti-clipping warnings, first complete compatibility with Virgo machines
0.1.3	*August 24*	beam-splitter, special surfaces, improved information on beams in graphical interface
1.0.0	Fall 2017	cavities, interferences, interface to beam tree navigation (interactive ghost beam hunting)

Table 3: The development schedule of `theia`. Dates in italic signify deadlines which have been met.

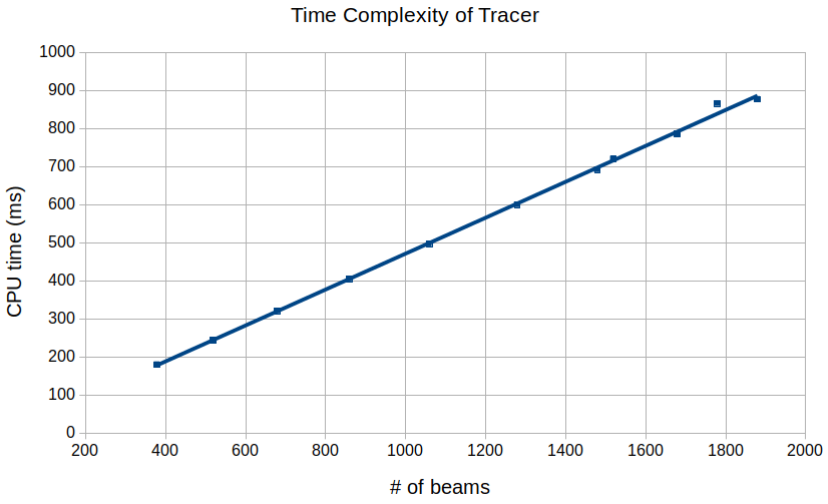

Figure 14: Time complexity of the tracing engine, as calculated on a i7/8GB processor.

5 Benchmarking and first steps

We will now evaluate the performances of the software and detail some of the first cases in which it proved useful.

5.1 Performances of the software

In order to evaluate the performances of the software, it is necessary to make calculations using the subparts of the program independently. The most critical part is the trace engine, which provides the gross of the data creation and serves the generated beams to the other parts of the software, such as the graphical CAD writer or the output text file writer.

In benchmarking the tracing engine, a test-case was written, and every call of the tracing engine was accounted for in terms of CPU time and of occupation of RAM, as a function of the number of beams traced through the setup.

Time complexity. Concerning the time complexity, the data are grouped in figure 14. As a linear fit, the CPU time was to be of 0.45 ms per traced beam with a correlation factor of 99.95% on the range of 400-1900 traced beams.

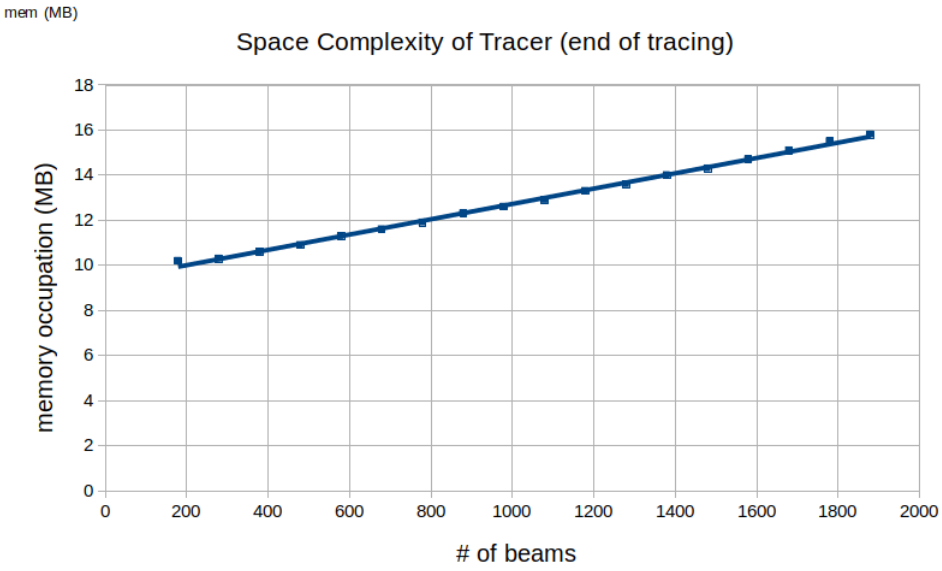

Figure 15: Space complexity of the tracing engine, as calculated on a i7/8GB processor.

Space complexity. The data for space complexity are grouped in figure 15. The RAM occupation was found to fit 9.3 MB of static occupation, plus 3.4 kB per beam on the range 200–1900 beams with a correlation coefficient of 99.76%.

The static occupation is linked to the simulation objects which exist independently of the traced beams, and to the stack of Python and its interpreter. This occupation is scarcely compressible, and will have a tendency to increase with time as more features and thus more static objects are added to the program.

Performances on large scales. Knowing the tracing algorithm as described in section 4.4, it is possible to estimate the number of beams traced in a typical Virgo-scale simulation, and thus to evaluate these performances in real-world cases.

- In the case where the simulation is limited by the threshold – we trace all the beams we can until the power decreases below the threshold, allowing an arbitrarily large strayness order – as it may be the case in stray light hunting, and if we estimate that every optic has two surfaces and considering balanced surfaces which have a 0.5 reflectivity, basic arithmetic shows that the number of traced beams is of the order of:

$$N = \frac{\text{input power}}{\text{threshold}}$$

  In the case of Virgo, simulations are scarcely limited by power and such estimations cannot be applied to real cases.

- In the case where the power is not limited, but the maximum order is fixed as in an optical design oriented simulation, the estimate is harder to evaluate. This is mainly because the number of optics also has to be taken into account. Nonetheless, we may claim that it is on the order of:

$$O(n^{\text{order}+1})$$

  Where order is the maximum order allowed by the simulation and n is the number of optics of the setup.

  In the case of Virgo, this is approximately 50 s, counting $n = 300$ optics in total and a order 1 simulation. 50 s for a global simulation of the instrument is acceptable.

5.2 Thermal lensing investigation at Virgo

The power accumulation in the Fabry-Perot cavities and the power recycling setup of the Virgo interferometer induce an absorption of heat by the optical components, and most importantly the mirrors of the cavities. By absorbing this thermal energy, the media undergo expansion, modifying the geometry of the optics and thus their optical properties such as focal lengths, etc. This effect is *thermal lensing*, and is common in gravitational interferometers.

The effect of thermal lensing is assessed by the beams of the external benches (at the end of the arms), which exhibit a widening of their waists. As explained in section 3.2, we resort to effective optics in order to determine the optical component the effect of which is analogous to the thermal lensing. Figure 16 shows the 3D rendering of such a simulation.

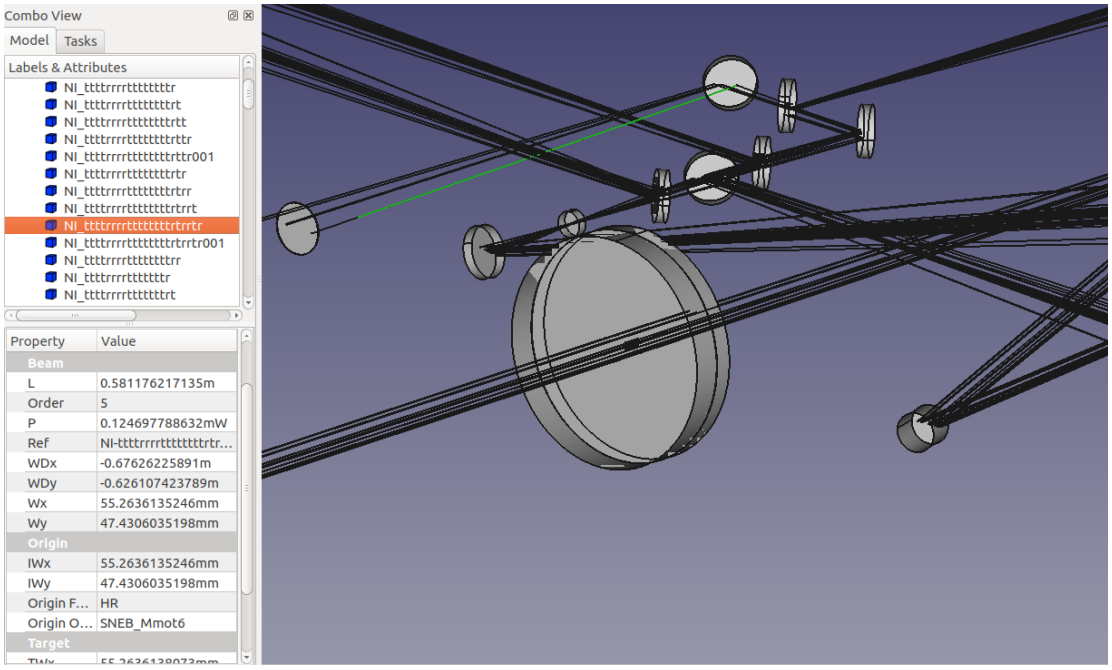

Figure 16: A screenshot of the CAD program reading the output file of `theia` after a simulation in the case of a thermal lensing investigation on the North End Bench of Virgo. Selecting a beam in the 3D view (green line) allows to analyze its Gaussian properties in the side panel (P:power, WDx, y: position of the waists along the beam, Wx, y: widths of the waists, Order: strayness order of the beam, Origin and Target: Gaussian data of the beam on its origin optic and upon impact on the target optic). This beam has an order of 5 because it has been transmitted by 5 mirrors, its power is on the order of $\sim$ nW. The beams emerging in the bottom left corner come directly from the end mirror of the North Fabry-Perot cavity.

To this effect, a configuration file is written for `theia` containing the relevant optics of the bench, and a script is written to vary the focal length of a lens placed along the path of the beam, immediately after the mirror showing thermal lensing (in this case the end mirror of the North Fabry-Perot cavity). This focal length is dynamically varied in order to reproduce the most faithfully the thermal lensing effect.

5.3 Optical bench designing

As a second illustration of the use of `theia`, let us consider a real-world case of optical bench design, though a very simple one. It will illustrate the scripting possibilities of our new software. The case may arise in the process of designing a telescope in order to match a beam to a cavity, as it is often the case at the optics laboratory of Virgo.

Let us consider two lenses of given focal lengths, and which must form a telescope together

as a single component. The first of the two lenses is fixed at a distance from the origin of the laser beam, and the second lens $L2$ has a variable position, along the bench (see figure 17). This position is precisely the variable we are going to optimize with `theia`, in order for example for the the beam emerging from the $L1 - L2$ ensemble to have the largest waist.

Figure 17: The setup of an optimization usage of `theia`, the position of $L2$ is varied in order for the waist of the final beam to be as large as possible.

We will use `theia` to generate the set of all waist sizes and positions of the final beam as the position of $L2$ is varied, then plot these results and deduce the optimal placement for $L2$. We will also notice that this optimal position coincides with the $2F$ configuration, i.e. when the lenses are two focal lengths apart.

The details of the script are not important, only the general algorithm, which we reproduce here:

1. Import the necessary modules from a plotting library and from `theia` for the tracing and Gaussian optics objects and functions;
2. Create a simulation object along with its threshold and maximum order parameters;
3. Create the original beam object, placed at the origin of the coordinate system and with the relevant properties for waists, etc.;
4. Create a lens of 20 cm focal length, placed 30 cm in front of the laser (these are the parameters for this particular simulation);
5. Create a set of positions for the second lens. Choose a variation interval around the $2F$ configuration for example, of a decent interval amplitude. For example: 50 positions between 40 cm − 2 cm and 40 cm + 2 cm;
6. For all the positions in the set of positions:

a. Create a lens at that position and load it into the simulation's set or optics;

b. Run the simulation, calculate the position and size of the waist of the out-coming beam;

c. Save those two results in a set for later plotting;

7. Plot the results;

The results for a 1 mm-waist input beam and 500 points between 38 cm and 42 cm for the second lens center are reported in figure 18. We find an optimal position of ~ 40.1 cm after $L1$. As expected, the optimal position is near the $2F$ configuration, and the position of the waist passes from behind the $L2$ continuously to in front of $L2$. If the input beam had been a plane wave, the waist size peak would have been narrower and the variation of the position of the waist more brutal.

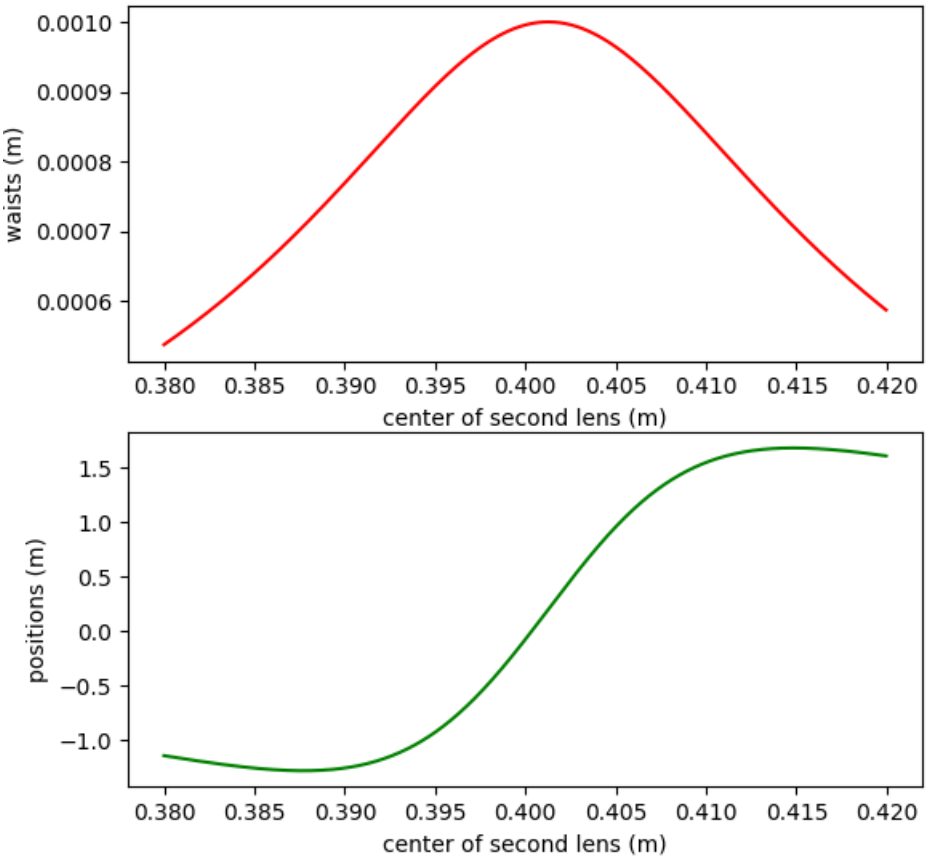

Figure 18: The sizes and positions of the waist of the output beam of the $L1 - L2$ configuration, as calculated by a `theia` script.

Conclusions and perspectives

`theia`, a new Gaussian beam tracer for gravitational observatories has been motivated and described. This new program benefits of an extensive user environment at `http://theia.hopto.org`. In its first use cases, it has exhibited simulation and scripting potential. Its testing carries on before the implementation of new features to meet even more closely the requirements of gravitational astronomy.

Of these, the priorities are the calculation of interferences, the simulation of cavities and the proper interface for stray light hunting.

References

[1] LIGO Scientific Collaboration and Virgo Collaboration: *Observation of Gravitational Waves from a Binary Black Hole Merger*, Phys. Rev. Lett. 116 (2016)

[2] LIGO Scientific Collaboration and Virgo Collaboration: *GW151226: Observation of Gravitational Waves from a 22-Solar-Mass Binary Black Hole Coalescence*, Phys. Rev. Lett. 116 (2016)

[3] LIGO Scientific Collaboration and Virgo Collaboaration: *GW170104: Observation of a 50-Solar-Mass Binary Black Hole Coalescence at Redshift 0.2*, Phys. Rev. Lett. 118 (2017)

[4] T. Damour: "Gravitational Waves and Binary Black Holes", *in* Séminaire Poincaré XXII, *Ondes gravitationelles* (2016)

[5] M. Maggiore: "Exploring the Universe with Gravitational Waves", *in* Séminaire Poincaré XXII, *Ondes gravitationelles* (2016)

[6] D. Shoemaker: "Detecting Gravitational Waves", *in* Séminaire Poincaré XXII, *Ondes gravitationelles* (2016)

[7] A. Einstein: *Naherungsweise Integration der Feldglieichungen der Gravitation*, Sitzungsberichte der Königlich Preußischen Akademie der Wissenschaften 688-696 (1916)

[8] L. Landau, E. Lifshitz: *Course of Theoretical Physics Vol. 2: The Classical Theory of Fields*, Butterworth–Heinemann (1975)

[9] A. Einstein: *Uber Gravitationswellen*, Sitzungsberichte der Königlich Preußischen Akademie der Wissenschaften 154 (1918)

[10] F. Dyson: "Gravitational Machines", *in A.G.W. Cameron, ed., Interstellar Communication*, Benjamin Press (1963)

[11] J. Weisberg, D. Nice, J. Taylor: *Timing Measurements of the Relativistic Binary Pulsar PSR B1913+16*, Astrophysical Journal 722 (2010)

[12] The Virgo Collaboration: *Advanced Virgo Technical Design Report* (2012)

[13] W.D. Arnett *et al.*, *Supernova 1987a*, Annual Review of Astronomy and Astrophysics 27 (1989)

[14] V. Savchenko, C. Ferrigno, S. Mereghetti, L. Natalucci, A. Bazzano *et al.*: *INTEGRAL upper limits on gamma-ray emission associated with the gravitational wave event GW150914*, The Astrophysical Journal Letters 820 (2016)

[15] M. Tavani, C. Pittori, F. Verrecchia, A. Bulgarelli, A. Giuliani: *AGILE Observations of the Gravitational Wave Event GW150914*, arXiv:1604.00955 (2016)

[16] V. Connaughton, E. Burns, A. Goldstein, M. Briggs, B.-B. Zhang *et al.*: *Fermi GBM Observations of LIGO Gravitational Wave event GW150914*, arXiv:1602.03920 (2016)

[17] The Virgo Collaboration: "VIRGO PROJECT", *in The Gravitational Voice, Special Anniverasry Edition*, 2009

[18] M. Maggiore: *Gravitational Waves. Vol. 2: Astrophysics and Cosmology*, Oxford University Press, under completion.

[19] LIGO Scientific Collaboration and Virgo Collaboration: *Prospects for Observing and Characterizing GW Transients with aLIGO and Advanced Virgo*, arXiv: 1304.0670 (2016)

[20] The KAGRA Collaboration: *Interferometer Design of the KAGRA GW Detector*, arXiv:1306.6747 (2013)

[21] E. Kochkina, G. Wanner, D. Schmelzer, M. Tröbs, G. Heinzel: *Modeling of the General Astigmatic Gaussian Beam and its Propagation through 3D Optical Systems*, Applied Optics 24 (2013)

[22] J, A. Arnaud, H. Kogelnik: *Gaussian Light Beams with General Astigmatism*, Applied Optics 8 (1969)

[23] `www2.mpq.mpg.de/ ros/optocad.html` (retrieved 06.2017)

[24] `https://granite.phys.s.u-tokyo.ac.jp/svn/LCGT/trunk/Tools/gtrace/` (retrieved 06.2017)

[25] `zemax.com` (retrieved 06.2017)